Digest Journal of Nanomaterials and Biostructures Vol. 17, No. 4, October-December 2022, p. 1431-1440

Enhanced the dielectric and energy storage properties of $BaZr_{1-x}Ti_xO_3$ lead-free ceramics

A. Ahmad[a], S. Uddin[b,c], M. F. Nasir[a], G. Dad[c], A. Zaman[a,*], V. Tirth[d,e]
[a]*Department of Physics, Riphah International University, Islamabad 44000, Pakistan*
[b]*Department of Physics, Government College Hayatabad, Peshawar 25000, Pakistan*
[c]*Department of physics, Qurtaba University of Science & Information Technology Peshawar 25000, Pakistan*
[d]*Mechanical Engineering Department, College of Engineering, King Khalid University, Abha 61421, Asir, Kingdom of Saudi Arabia*
[e]*Research Center for Advanced Materials Science (RCAMS), King Khalid University Guraiger, Abha 61413, Asir, P.O. Box No. 9004, Kingdom of Saudi Arabia*

Ferroelectric $BaZr_{1-x}Ti_xO_3$ ($0 \le x \le 8$) ceramic composition was synthesized by using solid state reaction method. The material was calcined at 1250 °C in air. In this work we have examined that the ferroelectric, energy storage and microwave dielectric properties of $BaZr_{1-x}Ti_xO_3$ at room temperature. The XRD patterns showed that $BaZr_{1-x}Ti_xO_3$ composition is of perovskite structure with a space group of Pm-3m. SEM morphology shows that increase in number of grain boundaries result in increase of polarisation. The energy storage properties were calculated from (P-E) loops by varying the electric field (range) and composition of the ceramic material. It has observed that the relative permittivity increases along with temperature. The storage energy density (W_{rec}) has been reported 0.043 J/cm^3, whereas efficiency (η) was 57% at room temperature and 40 kv/cm at contents (x=0.06).The Barium zirconium titanate (BZT) will be an excellent candidate material for storage energy devices.

(Received September 15, 2022; Accepted December 9, 2022)

Keywords: $BaZr_{1-x}Ti_xO_3$ perovskite, Solid state route, Ferroelectric, Energy storage, Pb-free

1. Introduction

Nowadays anyone faces the crises of any kind of energy and their demands of energy resources increases day by day. In next thirty years these demands should be doubled in throughout the world [1]. The natural resources coal oil and natural gas will nearly an end due to its big use. Which also creates pollution greenhouse-effects aerosols acid rain and global warming [2, 3]? Need to search for renewable energy resources, and to store these renewable energies which is an issue [4] Always these renewable energies are electrical in nature, so to store it [5] In the last decades, dipolar capacitors along with high energy storage density is the best choice among presently accessible to energy-storage equipment's i.e. batteries, dipolar capacitor, fuel battery cells and super capacitors [6-8]. Dielectrics have high energy storage (ES) materials due to their relatively large releasable energy density (*W*rec), high efficiency (η), and appropriate electric field breakdown strength (BDS) [9]. The energy density of the dielectric capacitors can be calculated by the area under the curve of equation,

$$\text{Wrec} = \int_{p_i}^{p_r} PdE \quad (1)$$

* Corresponding authors: zaman.abid87@gmail.com
https://doi.org/10.15251/DJNB.2022.174.1431

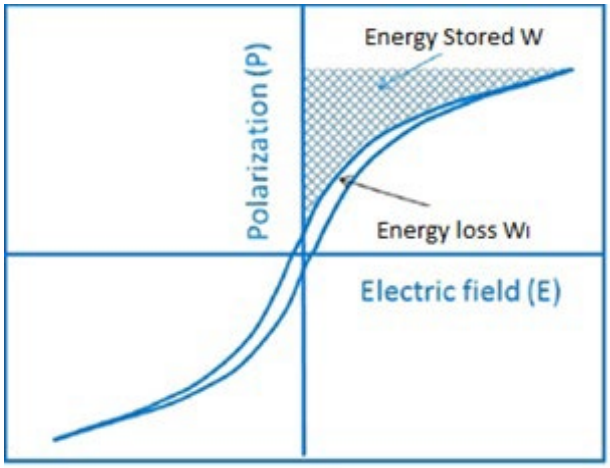

Fig. 1. The schematic diagram between electric field applied vs polarisation, energy loss and energy stored is shown in hysteresis loop and shaded area respectively.

In Eq.1 W_{rec} is the recoverable energy density which we will calculate from area in curve shown in shaded area, which is actually equal to the integral. From initial to saturated polarisation are renewable energy sources [10-12]. The efficiency of Energetic or smart material was investigated by the following equation.

$$\eta = \frac{W_{rec}}{W} \times 100\% \quad (2)$$

where η, W_{rec} and W are the high efficiency, releasable energy density and charging energy density respectively [13]. Majority of dielectric ceramics used for energy storage in capacitors are linear dielectrics ferroelectrics relaxer ferroelectrics and anti-ferroelectrics whose recoverable energy density can be achieved from figure 1 and equation 1[10-12].Due to environmental regulation lead free ceramics materials have mainstay research topic in recent days [14]. The researchers are working extensively on environment friendly materials following several regulations about the ban of hazardous materials and devices. Among Pb-free and environmentally friendly dielectric materials, Bi0.5Na0.5TiO3 (BNT) compositions are suitable alternatives for the application of energy storage devices and dielectric resonators [15, 16]. Venkata Srinivas Puli etal Lead-free (1 - x) BZT–xBCT sintered ceramics at sintering temperature (1600.0 °C), high relative permittivity along with low tangent loss was reported for the compound {Ba(Zr0.2Ti0.8)O3}(1-x){(Ba0.7Ca0.3)TiO3}x (x = 0.10, 0.15, 0.20) sintered ceramics. However, the electric breakdowns values i.e. (140, 170, 134 kV/cm) were recorded at 27°C (room temperature) while storage energy density i.e. (W_{rec} 0.88, 0.94, and 0.87 J/cm^3) [17]. Wenping Cao etal reported anti ferroelectric ceramics (lead free) of composition (1−*x*)[0.94NBT–0.06BT]–*x*ST. The maximum recoverable energy density of 0.98 J cm^{-3} with a relatively high efficiency of 82 % was achieved under 90 kV cm^{-1} at *x*=0.30, which also displayed excellent energy-storage stability in the temperature range from room temperature to 120 °C [18] Abid Ahmad et al. synthesized the composition (1–x)((Bi1/2Na1/2)0.94Ba0.06TiO3)–xBa1/2Sr1/2TiO3 (BNBT–BST),(0 < x > 0.1) sintered ceramics through sol–gel method. The storage energy density maximum values of energy density (0.57 J cm−3) and efficiency (43%) was recorded at 150.0 °C and 70.0 KV cm^{-1} respectively [19]. The dense BNT_BZT100x ,x=0.20,0.30,0.40,0.50 are fabricated by soled state sintering method exhibiting strong relaxer characteristics with energy storage density of 3.1j/cm^3 with 93% energy storage efficiency at 280kv/cm [20] In this study, La-doped Ba1-xLax(Zr0.25Ti0.75)O3 (BLZT, x = 0–8%) thin films were grown on LaNiO3 buffered Ca2Nb3O10-nanosheet/Si substrates. BLZT thin films with 5 mol.% La-doping simultaneously exhibit a great 72.2 J/cm3 recoverable energy-storage density and a large 78.6% energy-storage efficiency under a high 3.8 MV/cm breakdown strength [21]. The compound (NB1-xLxT-BZT-NN) (0.00 ≤ x ≤ 0.07) was synthesized by conventional method and it was observed the

breakdown field modified from ~115.0 to 137.0 kV cm^{-1} while the storage energy density increased from ~0.68 to 1.14 J cm^{-3} along with contents [22].

In this work, an effort is made to prepare the $BaZr_{1-x}Ti_xO_3$ lead free sintered ceramics ($0 \leq x \leq 0.8$) through mixed oxide route. We will reveal the effect of Ti^{+4} on the phase, microstructural, electrical and dielectric properties of $BaZrO_3$ materials by changing the operating frequency.

2. Experimental method

Ceramic composition of $BaZr_{(1-x)}Ti_xO_3$ ($0 \leq x \leq 0.8$) sintered ceramics were synthesized by conventional method. Solutions of research grade (>99% DAEJUNG Chemicals and materials Korea), Barium Carbonate $BaCO_3$ and Zirconium oxide $ZrCO_2$ and Titanium dioxide TiO_2 as raw material. Weight of Raw materials was done as required by stoichiometric ratios. The slurry of raw powders (polymer jar with propanol zirconia ball) was mixed and grinded by using horizontal ball milling for 12 hours. Overnight at 100ºC mixed solution was dried for 12 hours, the dried powder is grinded before calcination and put it in a crucible. Below melting temperature grind material $BaZr_{(1-x)}Ti_xO_3$ is calcinated at 1250 ºC at the rate of 50ºC/min. The choice of 1250ºC sintering temperature is determined by the growth of ceramics grains because there is a temperature point where the rate of grain growth increases sharply.

For the formation of pellets from the calcine powder was pressed by uni-axil press machine at 100.0 MPa pressure in a 10 mm diameter dye-disk shapes for the measurements of microwave dielectric and ferroelectric properties. $BaZr_{(1-x)}Ti_xO_3$ ($0 \leq x \leq 0.8$) samples (pellets) were sintered at 1500ºC temperature by using high energy furnace (Nabertherm GmbH, Germany) with heating/cooling rate of 50ºC/min with stay time 3 hrs at MRL (Material Research Laboratory), Institute of Physics, Peshawar University Pakistan. The structural and microstructural analysis were investigated by (Model JDX-3532) and (JEOL Japan) respectively. To measure ferroelectric and microwave dielectric properties of the silver paste samples was used impedance spectroscopy (Model CPE-1801). The microwave dielectric properties (temperature dependent) has been measured by using vector network analyser at different frequency range (1 KHz to 1 MHz). Poly K Ferroelectric Polarization loops and Dielectric Break down Test System Model CPE-1801 is used. By P-E hysteresis loop the energy storage density was measured indirectly.

3. Result and discussion

3.1. Structural and microstructural analysis

The XRD patterns of calcined sintered ceramic ($BaZrO_3$) shown cubic structure along with JCPDS card # 06-0399 along with space group (Pm-3m) as shown in the figure 2. The TiO_2 has been doped in $BaZrO_3$ ceramics might be because of the amalgamation of Ti^{4+} ion to 6-fold B-site cation coordination of perovskite structure relative to larger ionic radius of Zr^{4+} ion. The XRD analysis revealed that the crystallite size decreases by increasing the Ti^{4+} contents it is clear that to increased Ti content, the crystallite size has also decreased due to ionic radius of Zr^{4+} ion (0.87 Å) is greater than ionic radius of Ti^{4+} (0.68 Å) [23, 24]. By following the Braggs law ($2d\sin\theta=n\lambda$), the substitution of TiO_3 content at B-site cation may attributed the peak shifting [25].The Shifting of (1 1 0) plane toward higher 2θ values has been observed. The thermally etched samples of $BaZr_{1-x}Ti_xO_3$ ($0 \leq x \leq 0.8$) ceramics have been investigated.

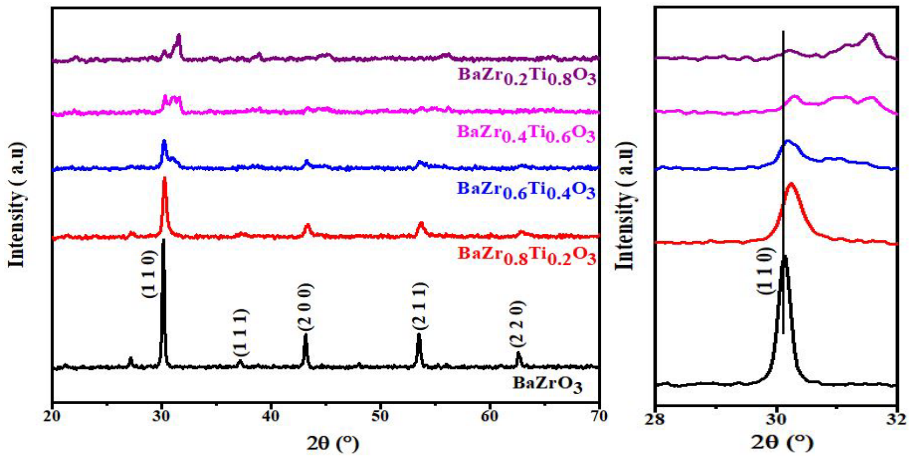

Fig. 2. (a) XRD pattern of $BaZr_{1-x}Ti_xO_3$ ($0 \leq x \leq 0.8$) ceramics. (b) Shifting of (1 1 0) plane toward higher 2θ values.

The effect of Ti^{+4} contents on the crystallite size of $BaZr_{1-x}Ti_xO_3$ structure ceramics which was evaluated by using Scherer's formula [26].

$$D = \frac{K\lambda}{\beta Cos\theta} \tag{3}$$

Where λ (1.5406 Å) shows the wavelength of X-ray, 'D' is the crystallite size and 'β' is the parameter of full width at half maximum (FWHM) measured in radian while 'θ' is the Braggs angle. Table 1 represented the average crystallite size, dislocation density and lattice strain. The values of lattice strain have been measured by using equation (4) [27].

$$\eta = \frac{\beta cos\theta}{4} \tag{4}$$

It was observed that the lattice strain increases with increasing Ti^{+4} contents (up to x=0.4) and then decreases. The change in the lattice strain and effects on the crystallite size was due to the difference of Radii of Zr^{4+} and Ti^{+4}.

The value of dislocation density has been measured by using equation (5) [28].

$$\delta = \frac{1}{D^2} \tag{5}$$

Where 'δ' is dislocation density while 'D' is the crystallite size. The variation of crystallite size, dislocation density and lattice strain along with Ti^{+4} contents as shown in Table 1.

Table 1. Physical properties of $BaZr_{1-x}Ti_xO_3$, ($0 \leq x \leq 0.8$) ceramics.

Contents (x)	D (nm)	δ ($x10^{-3}$ nm^{-2})	η ($x10^{-3}$)
0.0	453.7504	0.00486	0.000764
0.2	230.0914	0.01890	0.001507
0.4	102.3071	0.09550	0.003388
0.6	111.8462	8.9410	0.032776
0.8	39.86576	0.6290	0.008695

D= Average Crystallite size, δ= Dislocation density, η= Lattice strain

The secondary electron images (SEIs), from thermally etched and gold-coated of $BaZr_{1-x}Ti_xO_3$ ($0.00 \leq x \leq 0.80$) ceramics were investigated via SEM microscopy with magnification of 10,000 as shown in the Fig 3. All these samples are dense and have varying-microstructural topographies with the presence of holes. These holes represent some amount of porosity in the samples. The porosity decreases with increasing the relative density of the dopants elements. The shapes of grains of the samples were seemed to be spherical, faceted, and plate like. Moreover, the dissemination of grains has less identical [29]. The grain size also increases with increasing Ti^{+4} contents 'x'. The average grain size, D_{avg} could be estimated from the SEM images by using ImageJ software increase from 0.32 μm to 3.24 μm. The grain size and boundaries can be seen very clearly in the SEM images.

3.2. Phase Transition analysis

The solid solutions of $BaZr_{1-x}Ti_xO_3$ ($0 \leq x \leq 0.8$) samples phase Transitions were investigated via temperature dependent dielectric analysis, at different frequencies (i.e. 1 KHz, 10 KHz, 50 KHz, 100 KHz and 1 MHz).The variation of relative permittivity (ε_r) versus temperature shows spreading behaviour of curve. This spreading behaviour is explained by Maxwell-Wagner model, the material is said to be poor conductors have not cleared grain boundaries [30].

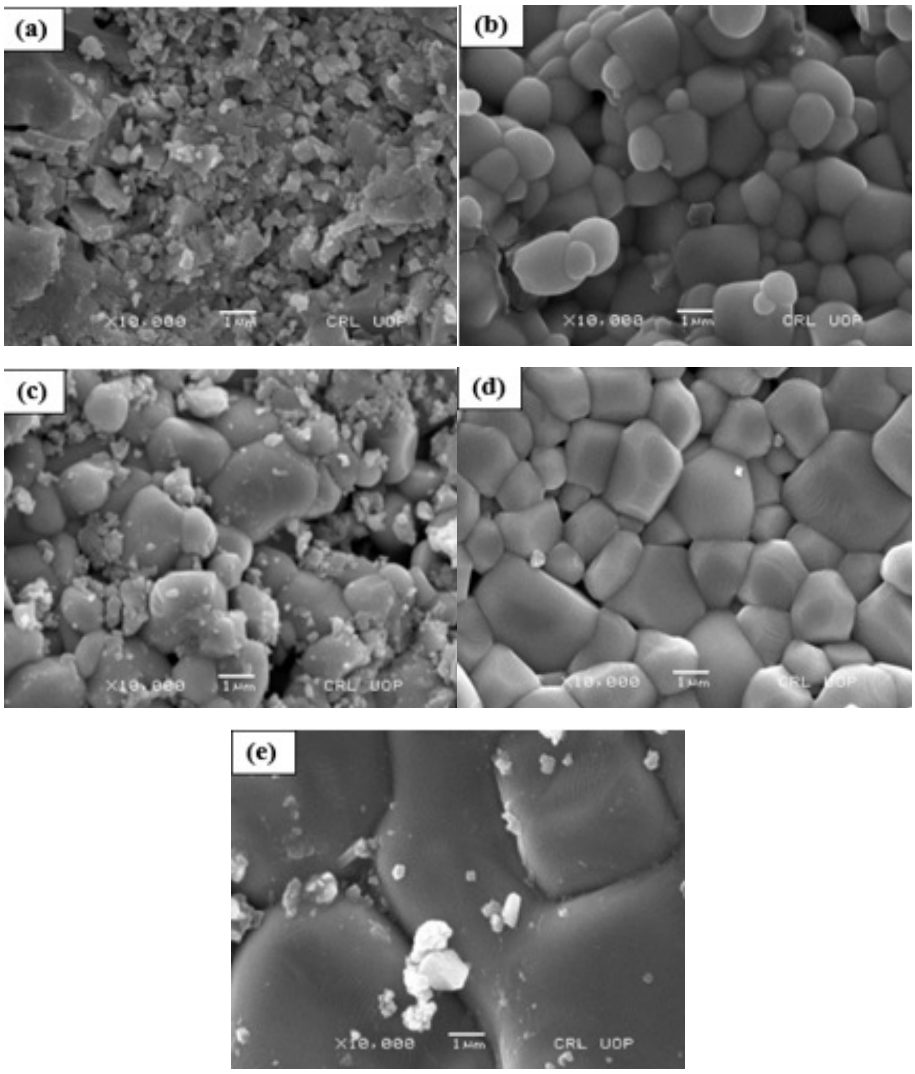

Fig. 3. SEM micrographs of $BaZr_{1-x}Ti_xO_3$ ($0 \leq x \leq 0.8$) of ceramics.

3.3. Microwave dielectric properties

Temperature dependent relative permittivity of $BaZr_{1-x}Ti_xO_3$ ($0 \leq x \leq 0.8$) sintered ceramics shown in Fig. 4(a-e). The frequency dependent relative permittivity's slowly increases along with increasing temperature till to Curie temperature (T_c), it might be trapped due to the movement of charge carriers. Due to increase of Ti contents in pure Barium Zirconate, defects in samples may be arise which may change the phase transition. The large number of electric dipole trapped due to defects in crystal produce an increasing in polarization and dielectric constant values. The value of relative permittivity has been changes along with operating frequency. Generally when frequency increases, the net polarizability decreases which further decreases the relative permittivity. The values of dielectric constant changes with Ti^{4+} content due to the difference in ionic radius of Ti^{4+} (~0.64 Å) and Zr^{4+} (~0.79 Å) [31].

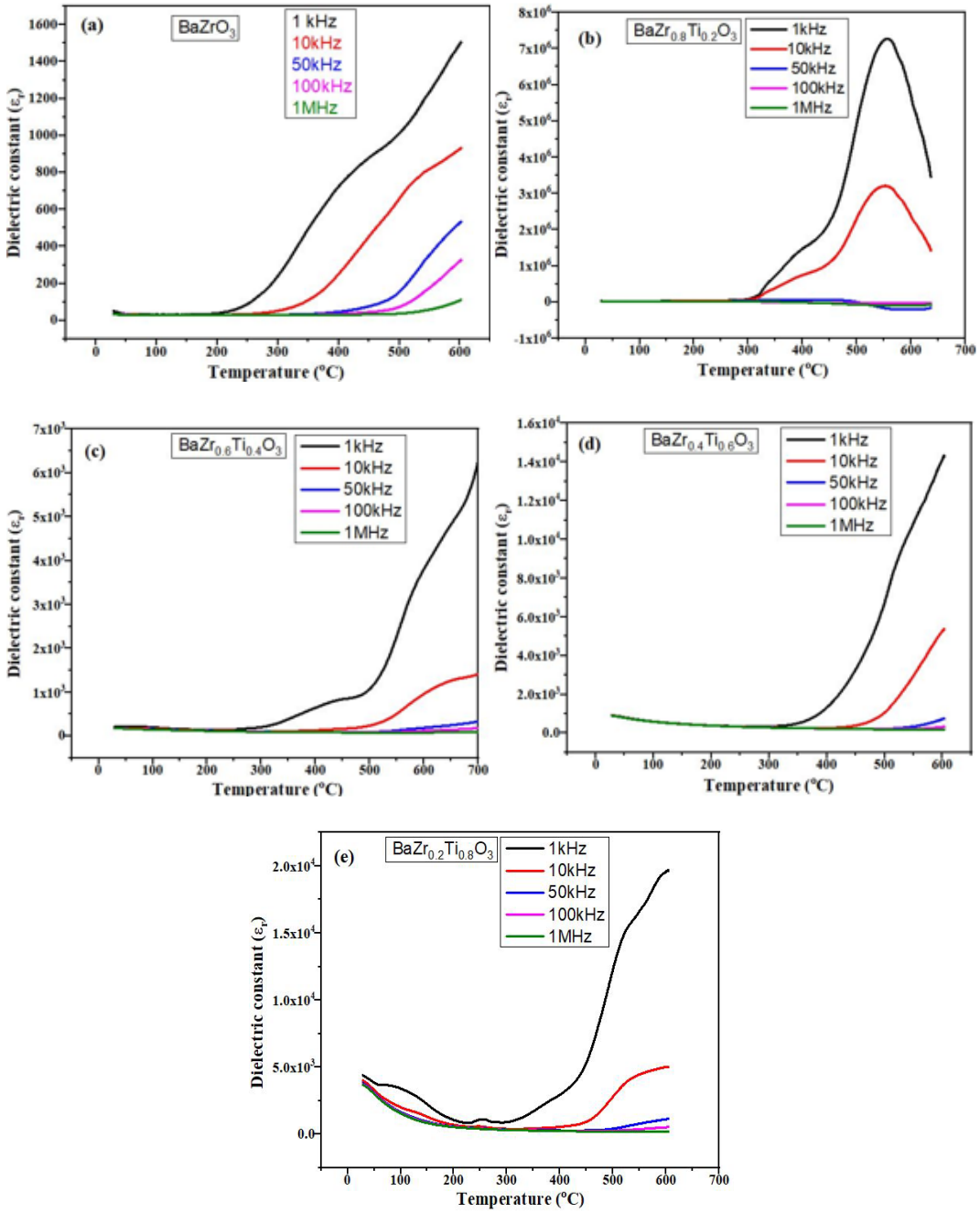

Fig. 4. (a), (b), (c), (d) and (e) shows variations of relative permittivity with frequency.

3.4. Ferroelectric properties

The frequency dependent ferroelectric properties of $BaZr1_{-x}Ti_xO_3$ ($0 \leq x \leq 0.8$) sintered ceramic as shown in the Fig. 5. The polarization plots versus electric field i.e. (PE- hysteresis) loops for all samples shown the variation of energy storage density and efficiency with increasing Ti contents. The recoverable energy density rises and PE- hysteresis loops become slim with increasing Ti contents. As the PE loops becomes slim it means that maximum polarisation increases P_{max}, also the remnant polarisation goes on increasing mood P_{rem} and the co-ercive field decreases. More polarisation can occur in concerned composition as we apply electric field in KV/cm and energy storage density increases. The doping of TiO_3 in $BaZrO_3$ causes the amalgamation of Ti^{4+} cation at 6-fold structure comparative to larger Zr^{4+} cation. The XRD pattern shown clearly that the crystallite size decreases with increasing Ti contents due to the differences of ionic radii [23, 32].

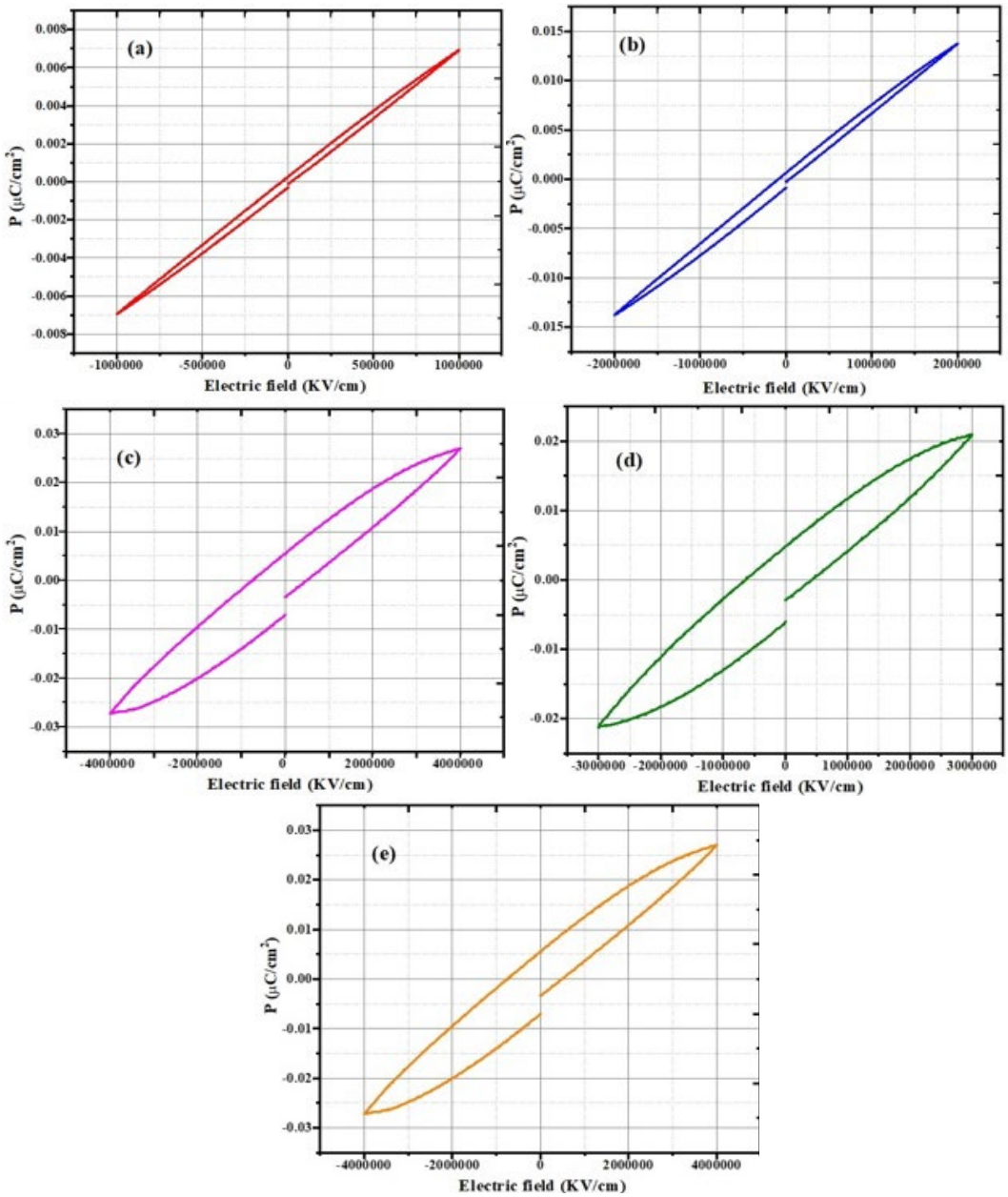

Fig. 5. (a) x=0.6 Electric Field=10KV/cm, (b) x=0.6 Electric Field 20KV/cm (c) x=0.6 Electric Field 30KV/cm (d) x=0.6 Electric Field 40KV/cm (e) x=0.6 Electric Field 50KV/cm are hysteresis loops between electric field applied vs polarisation.

Lead free (barium Zirconate titanate) based relaxer ferroelectrics, designed by introduction of $Bi(Zn_{0.5}Sn_{0.5})O_3$ with hetero-valent ion substitution with both sites cations changes to long range order, Nano Polar regions (NPR) persuades, and decrease the remnant-polarization (Pr).

The ceramic composite $(1-x)BZT–xBZS$ $(0.02 \leq x \leq 0.14)$ sintered ceramic synthesized by mixed oxide method. The ferroelectric relaxer feature of based sample slowly increases.

Increasing the BZS contents. Slim P–E loop was recorded at contents $x = 0.10$ & 0.14. A high Wreck-efficiency (η) of 2.16 J/cm^3, relatively attained in contents ($x = 0.10$) at 250.0 kV/cm (90.3% of the base sample) which was better than the reported BZT based sintered ceramics [33].

3.5. Properties for energy storage devices

The properties of $BaZr_{(1-x)}Ti_xO_3$ ceramic samples were deliberated by equation (1), from PE-loops for different compositions of BZT contents at several frequency and electric field. The maximum value of energy storage density (W) is 0.043 J/cm^3 was acquired at room temperature and the electric field 40kv/cm, and 57% efficiency at content ($x = 0.6$). Energy storage density has been recorded along with Ti contents. The Fig. 6 shown below between electric field and energy storage density shows us good behaviour of increasing electric field and an increase in storage with remnant polarisation of PE hysteresis loop. Also the Fig. 7 between electric field and efficiency shows us the behaviour of material with dopant.

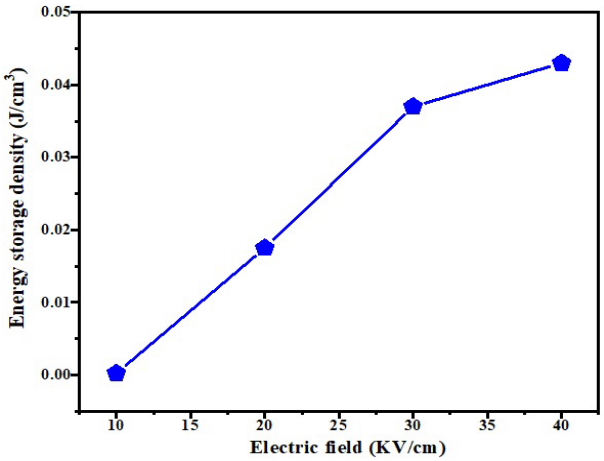

Fig. 6. Graph between electric filed applied and Energy storage density of different composition.

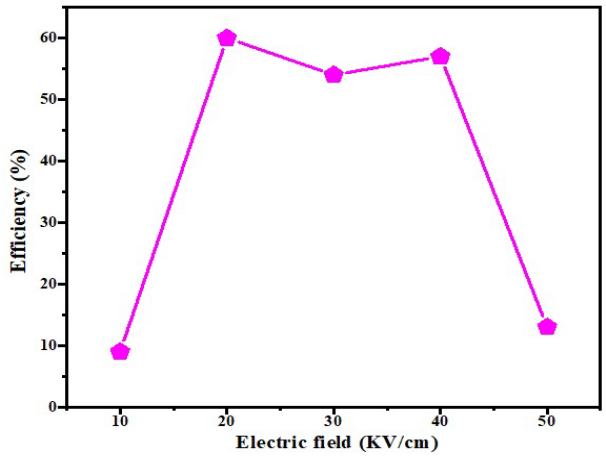

Fig. 7. Graph between electric Field applied vs efficiency of material different composites.

4. Conclusion

$BaZr_{1-x}Ti_xO_3$ ($0 \leq x \leq 0.8$) Single phase and dense perovskite structured composition ceramic were fabricated by solid state route method. XRD pattern revealed that the samples have cubical structure while SEM images shown spherical and plate like grains. The temperature dependent dielectric properties measured at different frequency were gradually increases upto Curie temperature (T_c). The ferroelectric and energy storage properties were measured at room temperature. The PE loop and its energy values calculated shows us that as we increase the Ti contents in $BaZrO_3$ the hysteresis loop squeeze and the remnant polarisation increased, and the crystallite size decreases. The storage Eenergy density (0.043 J/cm^3) and efficiency (57%) was recorded at content (x = 0.6). The lead free (BZT) is an excellent candidate material for the application of batteries or energy storage devices.

Acknowledgments

The authors extend their appreciation to the Deanship of Scientific Research at King Khalid University Abha 61421, Asir, Kingdom of Saudi Arabia for funding this work through the Small Groups Project under grant number RGP.1/74/42.

References

[1] Arnulf, G., (1999) Global Energy Perspectives: 2050 and Beyond. ENERGY Next Fifty Years, 41

[2] 2. Sherrill, S. A., Banerjee, P., Rubloff, G. W. & Lee, S. B., Phys. Chem. Chem. Phys. 13, 20714 (2011); https://doi.org/10.1039/c1cp22659b

[3] Ortega, N. et al., J. Phys. Condense. Matter 24 (2012); https://doi.org/10.1088/0953-8984/24/44/445901

[4] Burn I Smyth DM, Journal of material science 1972,7;339-43; https://doi.org/10.1007/BF00555636

[5] Amrit p. Sharma, J. Natureresearch 2019,9,16809; https://doi.org/10.1038/s41598-019-53358-0

[6] Chu, B. et al., Synthesis (Stuttg). 313, 2-5 (2006); https://doi.org/10.1126/science.1127798

[7]. Cao, Y. & Irwin, P. C., IEEE Trans. Dielect. Electr. Insul. 11, 797-807 (2004); https://doi.org/10.1109/TDEI.2004.1349785

[8]. Wen, L., Chen, J., Liang, J., Li, F. & Cheng, H. M., Natl. Sci. Rev. 4, 20-23 (2017); https://doi.org/10.1093/nsr/nww041

[9] Wang, T., Liu, J., Kong, L., Yang, H., Wang, F., & Li, C. (2020), Ceramics International, 46(16), 25392-25398; https://doi.org/10.1016/j.ceramint.2020.07.007

[10] Puli, V. S. et al., J. Mater. Sci. 48, 2151-2157 (2013); https://doi.org/10.1007/s10853-012-6990-1

[11] Burn, I. & Smyth, D., Ceramic. J. Mater. Sci. 7, 339-343 (1972); https://doi.org/10.1007/BF00555636

[12] Zhang, Q. et al., Appl. Phys. Lett. 109, 2-6 (2016); https://doi.org/10.1063/1.4973425

[13] Wang, Y., Wang, T., Wang, J., Liu, J., Xing, Z., Yang, H., ... & Li, C. (2021), Journal of the European Ceramic Society, 41(13), 6474-6481; https://doi.org/10.1016/j.jeurceramsoc.2021.05.052

[14] Zhao L Lui Q,Gau J,Zhang S,Li jF, Adv Materials 2017;29;1701824; https://doi.org/10.1002/adma.201701824

[15] Chen C S, Tu C S, Chen P Y, Ting Y, Chiu S J, Hung C, Lee H Y, Wang S F, Allen J A and Schmidt V 2014, Cry. Grow. 393 129-33; https://doi.org/10.1016/j.jcrysgro.2013.09.011

[16] Chaouchi A, Kennour S, Astorg S D, Rguiti M, Courtois C, Marinel S and Aliouat M 2011,

Alloy. Comp. 509 9138-43; https://doi.org/10.1016/j.jallcom.2011.06.085
[17] Venkata Srinivas Puli, Journal of Material Science (2013) 48:2151-2157; https://doi.org/10.1007/s10853-012-6990-1
[18] Wenping Cao et al., Ceramics, journal of energy technology 12 October 2015.
[19] Ahmad, A., Uddin, S., Zheng, G. P., & Nasir, M. F. (2021). Synthesis and temperature dependent energy storage characterization of (Bi1/2Na1/2) 0.94 Ba0. 06TiO3)–Ba1/2Sr1/2TiO3 ceramics. *Physica Scripta*, *96*(9), 095809.
[20] Yo Huong etal.(2019), Journal of Materiomics ,5;385-393; https://doi.org/10.1016/j.jmat.2019.03.006
[21] Minh D. ,(2021), "Nguyen Ultrahigh energy-storage performance in lead-free BZT thin-films by tuning relaxer behavior" 133,111072; https://doi.org/10.1016/j.materresbull.2020.111072
[22] Aqib Ali et al., Journal of material research Express 16 April 2021(1-9 page).
[23] Shanon RD 1976, Act. Cryst A32 751-67; https://doi.org/10.1107/S0567739476001551
[24] Chaouchi A, Kennour S, Astorg S D, Rguiti M, Courtois C, Marinel S and Aliouat M 2011, J. Alloy. Comp. 509 9138-43; https://doi.org/10.1016/j.jallcom.2011.06.085
[25] Chen C S, Tu C S, Chen P Y, Ting Y, Chiu S J, Hung C, Lee H Y, Wang S F, Allen J A and Schmidt V, 2014, J. Cry. Grow. 393 129-33; https://doi.org/10.1016/j.jcrysgro.2013.09.011
[26] Ali, A., Uddin, S., Iqbal, Z., Lal, M., Jameel, M. H., Zaman, A., & Khan, W. (2021), Journal of Materials Research and Technology, 11, 1828-1833; https://doi.org/10.1016/j.jmrt.2021.01.126
[27] Zaman, A.; Uddin, S.; Mehboob, N.; Tirth, V.; Algahtani, A.; Abbas, M.; Mushtaq, M.; Ali, A.; Sultana, F.; Althubeiti, K.; et al., 2022, ACS Omega, 7 (5), 4667-4676; https://doi.org/10.1021/acsomega.1c06918
[28] Zaman, A., Uddin, S., Mehboob, N., & Ali, A. (2020), Physica Scripta, 96(2), 025701; https://doi.org/10.1088/1402-4896/abce74
[29] Saini, D. S., Tripathy, S., Kumar, A., Sharma, S. K., Ghosh, A., & Bhattacharya, D. (2018), Ionics, 24(4), 1161-1171; https://doi.org/10.1007/s11581-017-2282-8
[30] Kremer F., & Schönhals A. (eds.), Broadband Dielectric Spectroscopy. - Springer-Verlage, 2003,ISBN 978-3-540-43407-8; https://doi.org/10.1007/978-3-642-56120-7
[31] Shannon, R. D., Acta Crystalloger. Sect. A Cryst. Phys. Diffract. Teor General Crystallogr. 32, 751-767 (1976); https://doi.org/10.1107/S0567739476001551
[32] Jha, P. A., & Jha, A. K. (2013), Journal of Materials Science: Materials in Electronics, 24(5), 1511-1518; https://doi.org/10.1007/s10854-012-0963-7
[33] Hameeda, O. M., Salem, B. I., Abdelfattah, H., Abdelfattah, G., & Shahab, M. (2019), Physica B: Condensed Matter, 574, 411680; https://doi.org/10.1016/j.physb.2019.411680